Section 2 Plasma Physics

Chapter 1. Plasma Dynamics

Academic and Research Staff

Professor George Bekefi, Professor Abraham Bers, Professor Bruno Coppi, Professor Jonathan S. Wurtele, Dr. Chiping Chen, Dr. Stefano Migliuolo, Dr. Abhay K. Ram, Dr. Linda E. Sugiyama, Ivan Mastovsky

Visiting Scientists and Research Affiliates

Dr. Giuseppe Bertin, Francesca Bombarda, Franco Carpignano, Dr. Carson C. Chow,[1] Dr. Paolo Detragiache, Dr. Vladimir Fuchs,[2] Dr. Eli Jerby,[3] Andrew J. Kerman, George M. Svolos, Dr. Jiri Ullschmied,[4] Dr. Ian Wilson,[5] Dr. Walter Wuensch[5]

Graduate Students

Abdulaziz Al-Jalal, James C. Blastos, Palmyra E. Catravas, Kai P. Chan, William S. Daughton, Darin R. Ernst, Wen Hu, Gregory E. Penn, Darren M. Pierre, Caterina Riconda, Todd H. Rider, Suraj D. Salihu, Steven D. Schultz, Gennady Shvets, Richard E. Stoner, Luigi Vacca, Pavel S. Volfbeyn

Undergraduate Students

Beth L. Chen, David Sisson

Technical and Support Staff

Felicia G. Brady, Catherine Lorusso,[6] Laura von Bosau, Miriam Weiner

1.1 Relativistic Electron Beams

Sponsors

U.S. Air Force - Office of Scientific Research
Grant F49620-93-1-0108
U.S. Army - Harry Diamond Laboratories
Contract DAAL02-89-K-0084
Contract DAAL02-92-K-0037
U.S. Department of Energy
Grant DE-FG02-91ER-40648
U.S. Navy - Office of Naval Research
Grant N00014-90-J-4130

Project Staff

Professor George Bekefi, Professor Jonathan S. Wurtele, Ivan Mastovsky, Dr. Chiping Chen, Dr. Eli Jerby, Dr. Jiri Ullschmied, Dr. Ian Wilson, Dr. Walter Wuensch, Abdulaziz Al-Jalal, James C. Blastos, Palmyra E. Catravas, Wen Hu, Gennady Shvets, Richard E. Stoner, Pavel S. Volfbeyn, Beth L. Chen, David Sisson

1.1.1 A 70-Period High-Precision Microwiggler for Free-Electron Lasers

Reducing the size and cost of visible and UV wavelength FEL systems is necessary to make them practical sources of radiation. The use of a short-period (1-10 mm) microwiggler magnet permits the generation of higher frequency radiation because the device is more compact than one employing wigglers of the usual period (typically 3-10 cm).

Microwiggler design and construction poses some very serious engineering challenges. Mechanical tolerances of a given value become increasingly

---

1 Boston University, Boston, Massachusetts.

2 Centre Canadien de Fusion Magnétique (CCFM), Quebec, Canada.

3 Tel Aviv University, Faculty of Engineering, Tel Aviv 69978, Israel.

4 Institute of Plasma Physics, Czechoslovak Academy of Sciences, P.O. Box 17, 18211 Prague 8, Czechoslovakia.

5 CERN, SL-RFL, CH-1211, Geneva 23, Switzerland.

6 Deceased, March 18, 1995.

large in the fractional sense as the size is reduced, leading to a corresponding increase in fractional field errors. Also, wiggler field strength falls off exponentially as the ratio of the separation between wiggler halves (the "gap") to the wiggler period increases. Therefore, maintaining a gap adequate to pass an electron beam (a few mm) while reducing the wiggler period results in significant field magnitude reduction unless corrective measures are taken.

Despite these difficulties, numerous groups have investigated short-period wigglers. A variety of techniques have been proposed and studied; some of these are: samarium-cobalt permanent magnet grooved slabs,[7] ferromagnetic core stacks with interleaved copper sheets,[8] high current pulsed-wire designs,[9] electromagnetic helical microwigglers,[10] staggered ferromagnetic core arrays immersed in a solenoidal field,[11] superconducting ferromagnetic core designs,[12] and hybrid samarium cobalt and iron microwigglers.[13] A common characteristic of most of these approaches is to control and minimize field errors by means of precise fabrication while dealing with steering errors (imparting of net transverse momentum to an electron beam) and deflection (imparting a net transverse displacement to an electron beam) with internal or external trim coils (note: Tecimer and Elias[13] used poleface shim tuning). These measures, while successfully employed in full-sized wigglers, have met with varying degrees of success in most of the above mentioned designs, yielding errors of order several percent RMS spread in the amplitudes of the wiggler field peaks, as well as uncompensated end effects (notable exceptions being Benzvi et al.,[12] having attained field errors of order 0.28 percent, and Tecimer and Elias[13] having achieved 0.2 percent; see table 1).

In contrast, we have constructed a 70-period planar microwiggler, having period 8.8 mm, which employs extensive tuning to accomplish field error reduction. Each half-period is independently adjustable, permitting great control over the amplitude profile. Also, we have developed a coil/ferrocore geometry permitting pulsed operation at high peak field amplitudes (4.2 kG) at experimentally useful repetition rates (> 1/2 Hz). The design is an outgrowth of our earlier work.[14]

We used amplitudes tuning to produce a 70-period microwiggler with 0.12 percent RMS spread in the peak amplitudes, the lowest value we are aware of in a sub-cm-period wiggler.

The microwiggler is a 70-period device with an 8.8 mm period and a 4.2 mm gap, consisting of 280 electromagnets held by a precisely formed aluminum matrix. Figure 1 illustrates the geometry of the microwiggler (and the coordinate axes used to describe the wiggler geometry).

---

[7] I. Kimel and R. Elias, "Micro-undulator Fields," *Nucl. Instr. Meth.* A296: 611-618 (1990); G. Ramian, L. Elias, and I. Kimel, "Micro-undulator FELs," *Nucl. Instr. Meth.* A250: 125-133 (1986).

[8] J.H. Booske, W.W. Destler, Z. Segalov, D.J. Radack, E.T. Rosenbury, J. Rodgers, T.M. Antonsen, Jr., V.L. Granatstein, and I.D. Mayergoyz, "Propagation of Wiggler Focused Relativistic Sheet Electron Beams," *J. Appl. Phys.* 64(1): 6-11 (1988).

[9] R.W. Warren, D.W. Feldman, D. Preston, "High-field Pulsed Microwigglers," *Nucl. Instr. Meth.* A296: 558-562 (1990).

[10] N. Ohigashi, K. Mima, T. Tsunawaki, S. Ishii, M. Ikeda, K. Imasaki, M. Fujita, S. Kuruma, A. Murai, C. Yamanaka, and S. Nakai, "Development of an Electromagnetic Helical Microwiggler," *Nucl. Inst. Meth.* A341: 426-430 (1994); J. Vetrovec, "Design of a High-field Taperable Helical Wiggler," *Nucl. Instr. Meth.* A296: 563-567 (1990).

[11] Y.C. Huang, H.C. Wang, R.H. Pantell, J. Feinstein, and J. Harris, "Performance Characterization of a Far-infrared, Staggered Wiggler," *Nucl. Instr. Meth.* A341: 431-435 (1994).

[12] I. Ben-Zvi, R. Fernow, J. Gallardo, G. Ingold, W. Sampson, and M. Woodle, "Performance of a Superconducting, High Field Subcentimeter Undulator," *Nucl. Instr. Meth.* A318: 781-788 (1992).

[13] M. Tecimer and L.R. Elias, "Hybrid Microundulator Designs for the CREOL Compact cw-FEL," *Nucl. Inst. Meth.* A341: ABS126-ABS127 (1994).

[14] R. Stoner, S.-C. Chen, and G. Bekefi, "A Planar Electromagnet Microwiggler for Free Electron Lasers," *IEEE Trans. Plasma Sci.* 18(3): 387-391 (1990).

GROUP	TECHNOLOGY AND STATUS	#PER.	λ_w/mm G/mm	B_w/kG	PEAK RMS ERROR	POLE INT. ERROR
Stoner *et. al.* MIT	Pulsed ferrocore electromagnet; operational	70	8.8/4.2	4.2	0.12%	0.18%
Huang *et. al.* Stanford	Staggered ferro-core array in solenoid; test	50	10.0/2.0	10.8	1.2%	Not reported
Warren and Fortgang LANL	Permanent magnet; operational	73	13.6/1.5	6.5	0.3%	Not reported
Tecimer and Elias CREOL	Hybrid; test	62	8/Not reported	1.0	0.2%	0.6%
Ben-zvi *et. al.* BNL	Superconducting ferrocore electro-magnet; test	20	8.8/4.4	>5.5	0.29%	0.36%

Table 1. Comparison of some short-period wigglers.

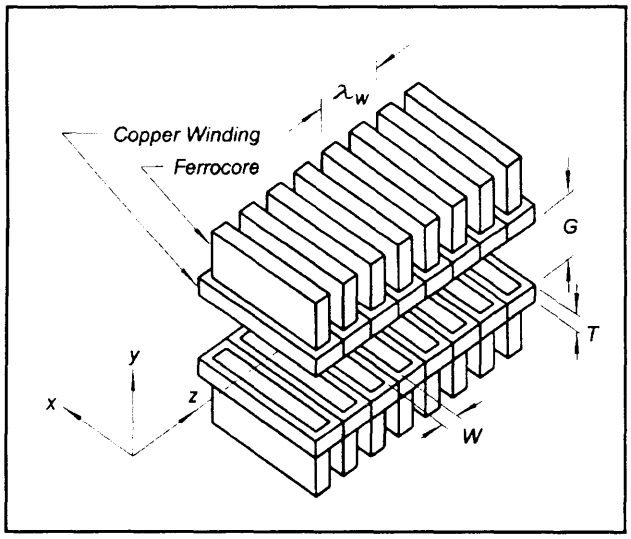

Figure 1. Microwiggler geometry. Coordinate axes are shown. Current flow in adjacent coils have opposite handedness, while current flow in cross-gap pairs have the same handedness. Parameter values: λ_w = 8.8 mm, G = 4.2 mm, T = 3.1 mm, W = 2.3 mm. Note that the gap shown is larger than in the actual design.

Figure 2 is a photograph of the microwiggler. Each electromagnet is formed from wire wound on a core consisting of six Microsil laminations of dimension 12.7 X 25.4 X 0.35 mm (29 gauge). Microsil was chosen in favor of more exotic materials (like vanadium permendur) because of its extremely low cost and ready availability, and its very small hysteresis and remnant fields. A very high degree of uniformity was achieved in the thickness of the laminated cores: the thicknesses of all 280 cores lay within a range between 2.101-2.106 mm. This precision was attained by sorting 2000 individual laminates according to thickness and then selecting sets of laminates having the proper total thickness. Figure 3 shows an individual electromagnet, which was hand wound with 50 turns of 32 AWG Formex wire.

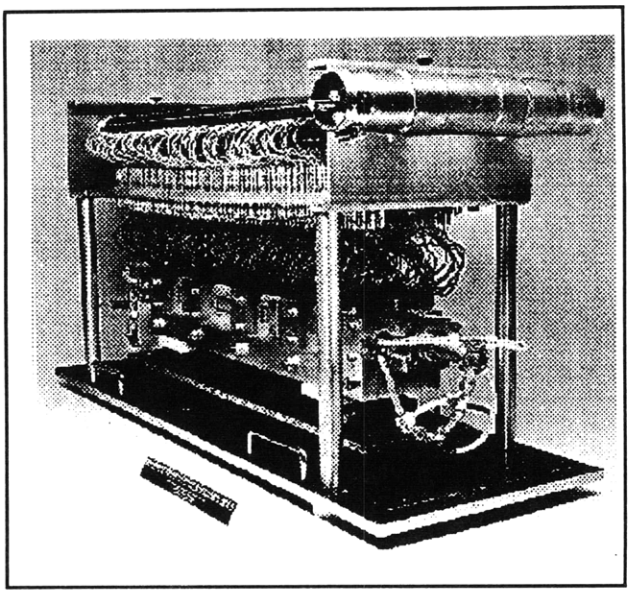

Figure 2. The Microwiggler. The high-current busswork (top) delivers 12 kA in 0.5 ms pulses, which is distributed by the current distribution network. Current is delivered to each of the 280 coils by a 22 AWG twisted pair.

The individual coils are placed in two aluminum holder pieces to form a wiggler configuration. Each holder consists of a bar fashioned from aluminum jig-plate stock with 140 slots cut perpendicular to the longitudinal axis of the bar: each slot accommodates an individual electromagnet. The two aluminum holder pieces lie on each side of the wiggler gap and are aligned by a pin-and-socket arrangement at each end of the holders.

The coil holders were manufactured with precision. Neither the width nor the cumulative (axial) positional error of any of the 140 coil holder slots in each holder exceeds 0.01 mm. The gap separation is determined by the aluminum holders. Figure 4 is a section drawing showing the assembly of the wiggler halves, drift tube, etc. The rectangular electron drift tube consists of a 75-cm length of 0.25-mm thick wall stainless steel K_a band waveguide with stainless mini-CONFLAT flanges braised onto each end. Longitudinal slots cut into each end of the magnet holders secure the drift tube position. The transverse position of the drift tube is also very well-fixed by the polefaces; this is crucial because the pickup coil probe for magnetic field measurements takes its position via a slip fit inside the drift tube. Measurement of the relative height of each of the 280 polefaces shows that the highest polefaces are randomly distributed through the wiggler and that they fix the transverse (y) position of the drift tube to better than 20 microns. Drift tube wall thickness variations thus yield as much (or more) drift tube position error as poleface height variations.

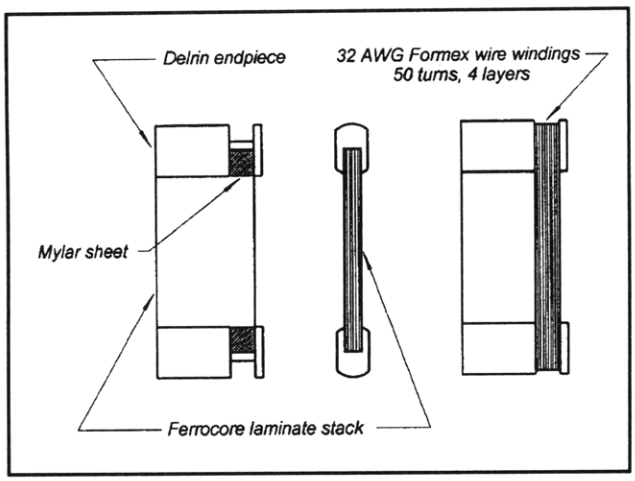

Figure 3. An individual electromagnet. The side view on the left shows a core without windings to better illustrate the structure of the core/endpiece assembly. The mylar sheet is indispensable: in tests, fully half of the coils made without it were electrically shorted to the core, a catastrophic failure rate.

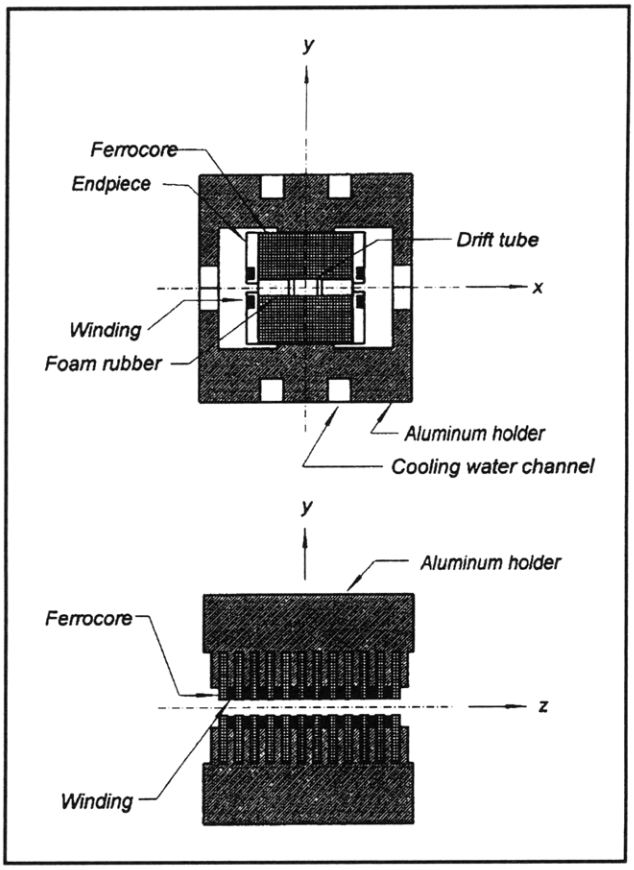

Figure 4. Wiggler assembly section drawings: (a) shows how the holders, coils, and drift tube are assembled. (b) illustrates the installation of the coils into the aluminum holders.

Two electromagnets facing across-gap from one another comprise a half-period and are connected in parallel to a ground and the current source through a tuning resistor. Figure 5 illustrates this arrangement schematically. The wiggler circuit consists of 140 half-period pairs, connected in parallel to the current source. Tuning is accomplished by means of variable resistors. They consist of 22 AWG manganin wires with their lengths varied to adjust their resistances. Tuning the microwiggler therefore consisted of adjusting the value of 140 resistors in a resistive current divider network. Care was taken to energize the microwiggler with pulses of long duration (880 μs) compared to the (L/R) time of the microwiggler (about 60 μs) to ensure that the impedance of the various half-period circuit elements remained primarily resistive.

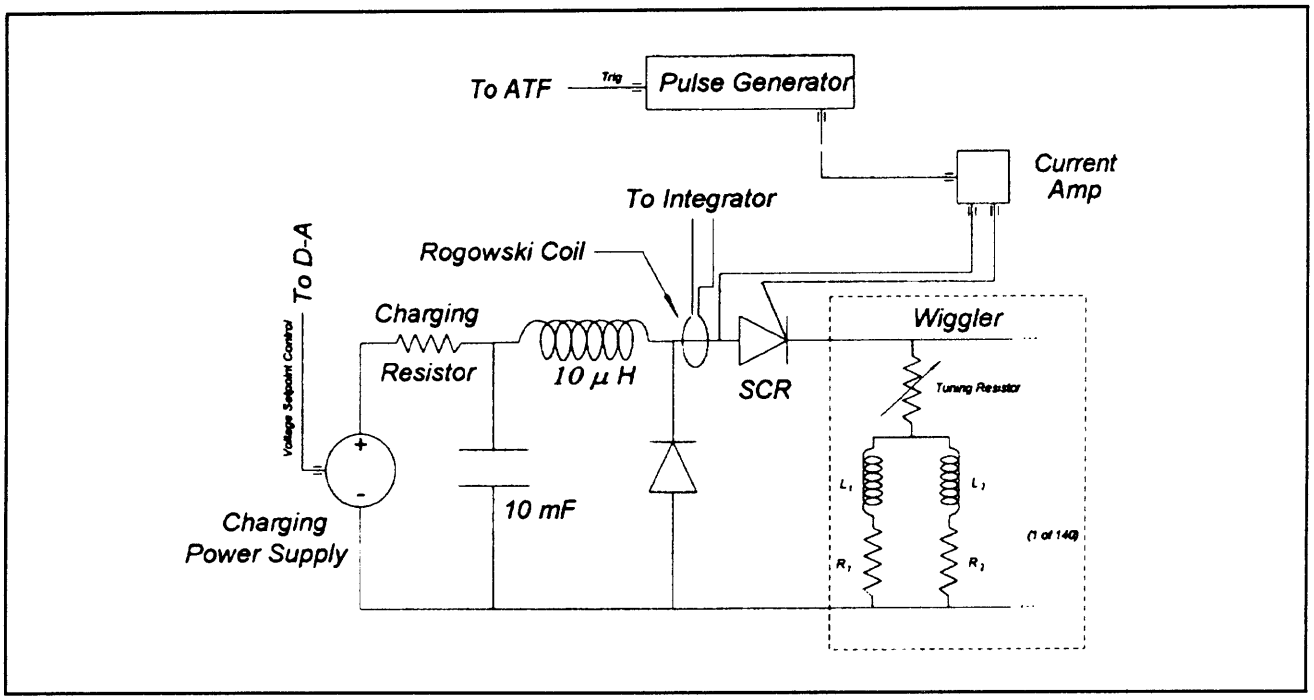

Figure 5. Schematic of the pulsed power supply for the microwiggler.

The measured peak amplitudes of our microwiggler are plotted in figure 6, as a function of peak number, before and after tuning. Two peaks at each end are tapered for minimal beam steering and deflection. A zero-steering POISSON model was generated, and the amplitudes obtained therefrom were tuned into the ends of the microwiggler. For these and all other measurements described in this section (the saturation data excepted), the microwiggler was operated at a repetition rate of 1/2 Hz and energized with underdamped half-sine waves of half-period 880 μs. The mean field amplitude was 4.2 kG.

In conclusion, we have constructed and operated a ferromagnetic-core based electromagnetic wiggler having 70 periods of 8.8 mm and a gap of 4.2 mm, producing an on-axis wiggler field of 4.2 kG in 0.5-ms pulses at a repetition rate of 0.5 Hz. We claim that the field produced has the smallest RMS spread in the peak amplitudes, 0.12 percent, and the smallest spread in the pole integrals, 0.18 percent, of any sub-cm-period wiggler yet reported. We have performed an extensive battery of measurements to support this claim. Our microwiggler is presently being used in a visible- and UV-wavelength FEL oscillator experiment at the Accelerator Test Facility, Brookhaven National Laboratory.

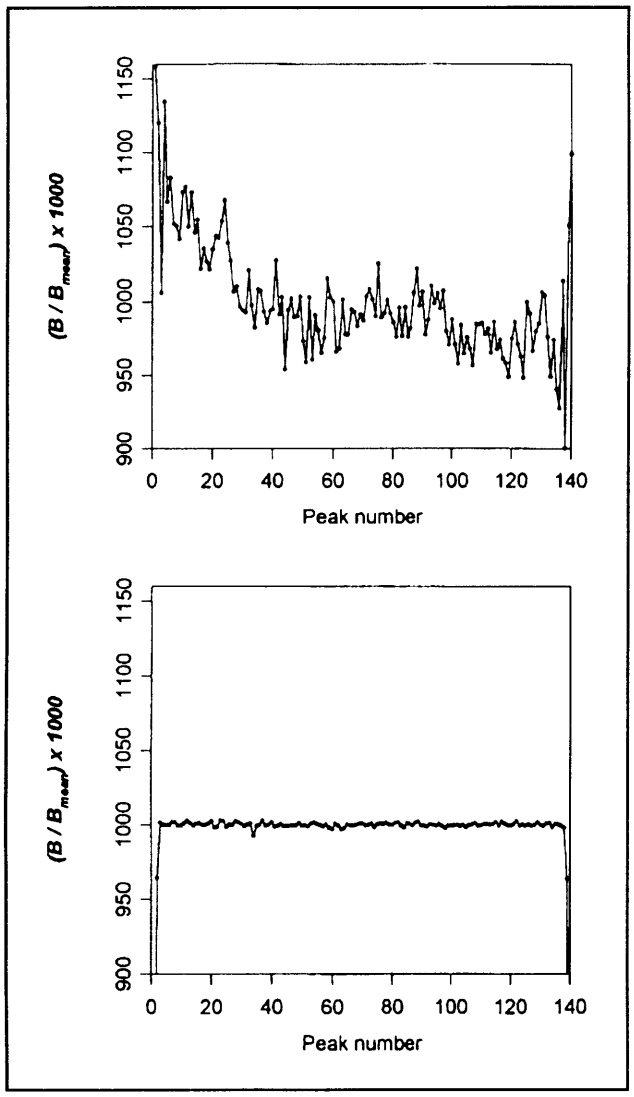

Figure 6. (a) Untuned and (b) tuned peak amplitude profiles of the microwiggler. The ranges and scales of the two plots are identical; clearly, tuning has greatly reduced peak amplitude variations. The tuned profile also shows the tapering of the end peaks.

1.1.2 Publications

Journal Articles

Bekefi, G., B. Chen, M.E. Conde, I. Mastovsky, K. Ricci, C.J. Taylor, and P. Volfbeyn. "Observations of Frequency Chirping and Phase of a Free Electron Laser Amplifier." *Nucl. Inst. Meth.* A341: 119-123 (1994).

Jerby, E., G. Bekefi, and A. Shahadi. "Observation of Chirping in a Traveling-Wave Cyclotron Maser Experiment." *Nucl. Inst. Meth.* A341: 115-118 (1994).

Jerby, E., A. Shahadi, V. Grinberg, V. Dikhtiar, M. Sheinin, E. Agmon, H. Golombek, V. Trebich, M. Bensal, and G. Bekefi. "Cycltron Maser Oscillator Experiments in a Periodically Loaded Waveguide." *IEEE J. Quantum Electron.* Forthcoming.

Stoner, R., and G. Bekefi. "A 70-Period High-Precision Microwiggler for Free Electron Lasers." *IEEE J. Quantum Electron.* Forthcoming.

Volfbeyn, P., K. Ricci, B. Chen, and G. Bekefi. "Measurement of the Temporal and Spatial Phase Variations of a Pulsed Free Electron Laser Amplifier." *IEEE Trans. Plasma Sci.* 22(5): 659-665 (1994).

Theses

Blastos, J.C. *The Spectral Analysis of the Spontaneous Emission of MIT's 8.8 mm, Room Temperature, Pulsed Free Electron Laser Microwiggler.* S.M. thesis, Dept. of Phys., MIT, 1994.

Catravas, P.E. *MIT 3.3 GHz Relativistic Klystron Amplifier: Experimental Study of Input Cavity and Beam Characteristics.* S.M. thesis. Dept. of Electr. Eng. and Comput. Sci., MIT, 1994.

Chen, B.L.-J. *Experimental Studies of a CERN-CLIC 32.98 GHz High Gradient RF Accelerating Structure Driven by a Free Electron Laser Amplifier.* B.S. thesis. Dept. of Phys., MIT, 1994.

Hu, W. *Generation of Coherent High-Power Microwave Radiation with Relativistic Electron Beams.* S.M. thesis. Dept. of Phys., MIT, 1994.

Shvets, G. *Interaction of Intense Lasers with Plasmas.* Ph.D. diss., Dept. of Phys., MIT, 1994.

Sisson, D.L. *Magnetic Field in a Tunable Microwiggler.* B.S. thesis. Dept. of Phys., MIT, 1994.

Stoner, R.E. *Radiation from Relativistic Electron Beams in Periodic Structures.* Ph.D. diss. Dept. of Phys., MIT, 1994.

Volfbeyn, P.S. *Measurements of the Temporal and Spatial Phase Variations of a 33 GHz Pulsed Free Electron Laser Amplifier and Application to RF Acceleration.* S.M. thesis, Dept. of Phys., MIT, 1994.

1.2 Plasma Wave Interactions—RF Heating and Current Generation

Sponsors

National Science Foundation
Contract ECS 94-42438
U.S. Department of Energy
Grant DE-FG02-91-ER-54109

Project Staff

Professor Abraham Bers, Dr. Abhay K. Ram, Dr. Carson C. Chow, Dr. Vladimir Fuchs, Kai P. Chan, Steven D. Schultz, Luigi Vacca

The research work of this group is concerned with studies on the electrodynamics of plasmas. Attention is directed toward understanding the nonlinear dynamics of plasmas driven by high-frequency electromagnetic fields (such as in RF heating and current drive of magnetically confined plasmas, or as in laser-plasma interactions), and the generation and propagation of unstable radiations from laser-plasma interactions and anisotropic electron distributions in space and astrophysical plasmas.

In the following, we report on our continuing studies to determine the conditions for optimizing power mode conversion of fast Alfvén waves to ion-Bernstein waves. These studies form the basis for using ion-Bernstein waves as a means of enhancing current drive efficiency in advanced tokamak scenarios.[15] The second report is on some initial progress in understanding the effect of RF waves on the bootstrap current in a tokamak. The third report gives some of the recent results on the orbits of energetic ions interacting with RF waves in the ion cyclotron range of frequencies. These calculations are the basis of our studies to determine the RF-induced transport of energetic ions.

1.2.1 Mode Conversion of Fast Alfvén Waves to Ion-Bernstein Waves

Sponsor

U.S. Department of Energy
Grant DE-FG02-91-ER-54109

In tokamak plasmas heated by waves in the ion-cyclotron range of frequencies (ICRF), the power is carried from the antenna into the center of the plasma by fast Alfvén waves (FAW). Near the ion-ion hybrid resonance inside the plasma, the FAW can couple to ion-Bernstein waves (IBW). These IBWs interact effectively with electrons and can lead to electron heating[16] or, in the presence of lower-hybrid current drive (LHCD), enhance the current drive efficiency.[17] The latter case explained observations on JET of the enhancement in LHCD efficiency in the presence of ICRF heating. The observed conditions required for this enhancement also are the conditions for which a fraction of the incoming power can be mode-converted to IBWs. This was discussed in the previous *RLE Progress Report.*[15]

Our previous results[17] have shown that the IBWs propagate short distances away from the mode conversion region before they are damped on electrons. Thus, by moving the mode conversion region in a plasma, one can control the spatial location where the IBWs transfer their energy and momentum to the electrons. We have also found that the electron diffusion coefficient in the presence of IBWs is significantly larger than in the presence of FAWs.[15] Recent experiments on TFTR have shown substantial electron heating near the mode conversion region. Furthermore, the region heating changes with a change of the location of the mode conversion region. From these observations, it has been concluded that the heating is due to mode converted IBWs. It has also been observed on TFTR that the directionality of the FAW spectrum is maintained by the IBWs after mode conversion. Currents were generated in the plasma near the mode conversion region when an

---

[15] A. Bers, A.K. Ram, C.C. Chow, V. Fuchs, K.P. Chan, S.D. Schultz, and L. Vacca, "Plasma Wave Interactions—RF Heating and Current Generation," *RLE Progress Report* 136: 237-249 (1993).

[16] A.K. Ram and A. Bers, *Phys. Fluids* B3: 1059 (1991).

[17] A.K. Ram, A. Bers, S.D. Schultz, and V. Fuchs, "Interaction of Ion-Bernstein Waves with Electrons," *Bull. Am. Phys. Soc.* 39: 1626 (1994); A.K. Ram, A. Bers, S.D. Schultz, and V. Fuchs, "Enhanced Current Drive with Lower-Hybrid and Ion-Bernstein Waves," *Proceedings of the 15th International Conference on Plasma Physics and Controlled Nuclear Fusion Research (IAEA),* Seville, Spain, September 26 - October 1, 1994, forthcoming; A.K. Ram, A. Bers, V. Fuchs, and S.D. Schultz, "Current Drive by the Combination of Lower Hybrid and ICRF Waves," *Proceedings of the 21st European Physical Society Conference on Controlled Fusion and Plasma Physics,* Montpellier, France, 3: 1134-1137 (1994); A.K. Ram, A. Bers, V. Fuchs, and S.D. Schultz, "Enhancing Lower Hybrid Current Drive with ICRF Waves," *Proceedings of the International Sherwood Fusion Theory Conference,* Dallas, Texas, March 14-16, 1994, paper 1C49.

asymmetric FAW spectrum was launched by the antenna. This indicates that IBWs could also be used for current drive. Since ICRF-generated heating and current drive is expected to play an important role in the future tokamaks (TPX and ITER), we have been examining the possible use of mode converted IBWs in advanced tokamak scenarios.

There are three important issues that need to be studied so that we can determine the importance of IBWs in advanced tokamak scenarios. The first issue is to determine the fraction of the incident FAW power that can be coupled to IBWs and the conditions for which the mode converted power can be maximized. The second issue is to determine the trajectories of the IBWs after mode conversion and the spatial location where the IBWs will interact with the electrons. The third and final issue is to determine the effectiveness of this interaction. In particular, for the case of current drive by IBWs, we need to know the efficiency of current drive by IBWs. Here we report on some of the recent progress we have made towards determining the conditions for optimizing the mode conversion to IBWs.

For efficient mode conversion of the ICRF-FAW power to IBWs, the fundamental ion cyclotron layers should be near the edge or outside the plasma, and the ion-ion hybrid resonance (IHR) layer should be in the central region of the plasma. In the simplest, one-dimensional (equatorial plane) description of the FAW, the local cold-plasma dispersion relation is:

$$n_\perp^2 = \frac{(L - n_\parallel^2)(R - n_\parallel^2)}{S - n_\parallel^2} \qquad (1)$$

where $n_\perp = ck_\perp/\omega$, $n_\parallel = ck_\parallel/\omega$, c is the speed of light, $k_\parallel$ is the component of the wave vector along the toroidal magnetic field, $k_\perp$ is the component of the wave vector perpendicular to the toroidal magnetic field, ω is the ICRF frequency, and S, R, L are the usual Stix tensor elements. $R = n_\parallel^2$ gives the positions of the right-hand cutoffs (RHC). There are usually two such cutoffs: one on the low magnetic field side (LFS) near the antenna, and another on the high magnetic field side (HFS) near the inside edge of the plasma. The positions where $L = n_\parallel^2$ and $S = n_\parallel^2$ correspond to the left-hand cutoff (LHC) and IHR, respectively. Usually, the LHC and the IHR are close to each other and define the Budden-type cutoff-resonance pair. In the vicinity of this region, local analysis leading to (1) breaks down and the propagation of FAWs is described by a differential equation:

$$\frac{d^2E_y}{dx^2} + Q(x)E_y = 0 \qquad (2)$$

where E_y is the normalized (poloidal) component of the electric field, x is the normalized spatial coordinate along the equatorial plane, and Q(x) is the potential function,[18] which for a cold plasma is equal to the right-hand side of (1). The Budden-type analysis of the mode conversion process only includes the LHC and the IHR. For such a cutoff-resonance pair we can express Q(x) in a simple form:

$$Q(x) = \gamma - \frac{\beta}{x} \qquad (3)$$

where γ and β are chosen to fit the right-hand side of (1) near the IHR and LHC. (In this model the IHR is located at x = 0 and the LHC is located at $x = \beta/\gamma$.) The solution to (2) with the model potential given in (3) can be written in terms of the Whittaker functions.[19] An asymptotic analysis of the Whittaker functions will completely determine the scattering parameters. From such an analysis, it has been found[20] that the power transmission coefficient is:

$$T_B = e^{-\pi\eta} \text{ where } \eta = \frac{\beta}{\sqrt{\gamma}}. \qquad (4)$$

The power reflection and power mode conversion coefficients are, respectively,

$$R_B = T_B(1 - 2T_B) \text{ and } C_B = T_B(1 - T_B). \qquad (5)$$

Thus, the maximum power mode conversion coefficient can be only 25 percent, i.e., from the Budden-type analysis of the mode conversion process, under ideal circumstances, a maximum of 25 percent of the incoming FAW power can be converted to IBWs.

---

[18] C.N. Lashmore-Davies, V. Fuchs, G. Francis, A.K. Ram, A. Bers, and L. Gauthier, *Phys. Fluids* 31: 1614 (1988).

[19] M. Abramowitz and I.A. Stegun, *Handbook of Mathematical Functions* (New York: Dover Publications, 1972).

[20] K.G. Budden, *The Propagation of Radio Waves* (Cambridge, Massachusetts: Cambridge University Press, 1985), pp. 596-602.

However, the Budden potential (3) does not account for the reflection of the FAW at the HFS-RHC. This can significantly modify the mode conversion results obtained from the Budden potential. An easy way to see the effect of the HFS-RHC is as follows. We assume that the potential function is still represented by the Budden potential (3). However, we impose an additional condition: we assume that the wave incident from the low field side ($x > 0$), after passing through the LHC-IHR cutoff-resonance pair, is completely reflected at some point $x = x_R (x_R < 0)$ where x_R is the location of the HFS-RHC. Clearly, in this case the transmission coefficient is zero, since the waves do not propagate for $x < x_R$. Thus, we only have a power reflection coefficient and a power mode conversion coefficient. The general solution, in terms of the Whittaker functions, is given by:

$$E_y(x) = c_1 W_{\kappa,\mu}(z) + c_2 W_{-\kappa,\mu}(-z) \tag{6}$$

where c_1 and c_2 are arbitrary constants that depend on the boundary conditions, and

$$z = -2i\sqrt{\gamma}\,x, \quad \kappa = -\frac{i}{2}\frac{\beta}{\sqrt{\gamma}} = -\frac{i}{2}\eta, \quad \mu = \frac{1}{2}. \tag{7}$$

For $x \to -\infty$, $W_{\kappa,\mu}(z)$ represents an incoming (towards $x = 0$) wave while $W_{-\kappa,\mu}(-z)$ represents an outgoing wave. If we assume that there is no damping of the wave between the resonance and the high-field cutoff, then c_1 and c_2 differ by at most an arbitrary phase. Let us assume that $c_2 = c_1 \exp\{-i(\pi + \phi)\}$. Then, using the asymptotic properties of the Whittaker functions for $x \to \infty$, the power reflection coefficient is:

$$R = \left| \frac{e^{i\sqrt{\gamma}\,x} e^{\pi\eta/4} |2\sqrt{\gamma}\,x|^{-i\eta/2} \left\{ 1 - e^{-i(\pi+\phi)} \dfrac{2\pi i e^{\pi\eta/2}}{\Gamma(-i\eta/2)\Gamma(1-i\eta/2)} \right\}}{e^{-i(\pi+\phi)} e^{-i\sqrt{\gamma}\,x} |2\sqrt{\gamma}\,x|^{-i\eta/2} e^{3\pi\eta/4}} \right|^2 . \tag{8}$$

Using the properties of the Gamma function,[19] it can be shown that:

$$R(\eta, \phi) = (1 - T_B)^2 + T_B^2 - 2T_B(1 - T_B)\cos(\phi + 2\psi)$$

$$= 1 - 4T_B(1 - T_B)\cos^2\left(\frac{\phi}{2} + \psi\right) \tag{9}$$

where T_B is given in (4), and ψ is the phase of $\Gamma(-i\eta/2)$. Then the power-mode conversion coefficient is:

$$C(\eta, \phi) = 4T_B(1 - T_B)\cos^2\left(\frac{\phi}{2} + \psi\right). \tag{10}$$

The maximum power mode conversion coefficient can now be 100 percent provided $T_B = 1/2$ and the $\phi/2 + \psi$ is an integer multiple of π. Thus, the effect of a high-field side reflection in the Budden problem can significantly alter the power mode conversion coefficient. In figure 7 we have plotted contours of constant $C(\eta, \phi)$ as functions of ϕ and η. These contours are periodic in ϕ modulo 2π. From this figure, it is clear that the maximum value of C is critically dependent on η—the distance between the left-hand cutoff and the ion-hybrid resonance.

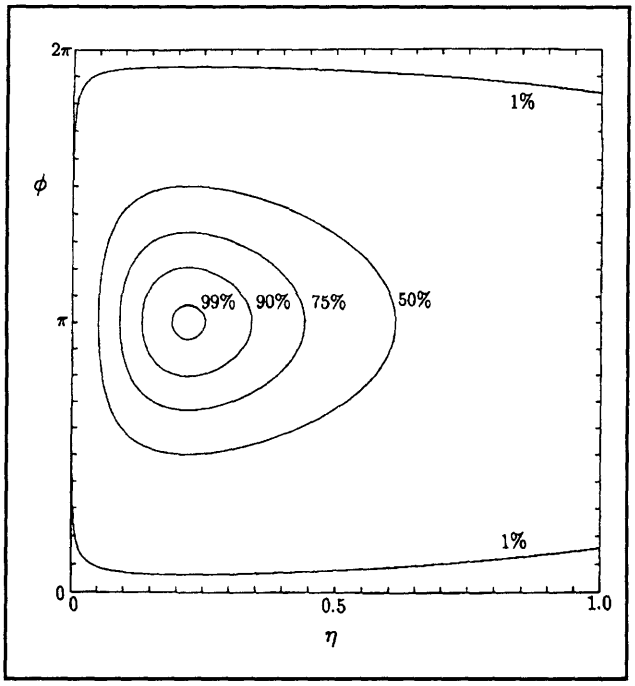

Figure 7. Theoretical contours of percent power mode converted in the (ϕ, η) plane; the figure is 2π-periodic in ϕ. These are contours of maximum possible power mode conversion coefficient. For large conversion (small reflections) the range of η's is relatively narrow.

For example, for $\eta > 0.3$ it is not possible to get 100 percent mode conversion regardless of the choice of the phase ϕ.

The physics leading to this enhanced mode conversion due to the HFS-RHC is similar to the behavior of a transmission line coupled to a dissipative resonator: complete absorption results when the incident FAW is critically coupled to the resonator formed by the LHC-IHR-RHC plasma system; the HFS-RHC adjusts the resonator while the LHC-IHR adjusts the coupling.

Studies are presently underway to determine the dependence of ϕ on plasma parameters. Recently, we have used the phase-integral technique[21] to find ϕ. We are also applying our results to determine the optimum mode conversion regimes in Alcator C-MOD, Tore Supra, and TPX.

1.2.2 Enhancement of the Bootstrap Current in Tokamaks Using RF Waves

Sponsors

Magnetic Fusion Science Fellowship Program
National Science Foundation
Grant ECS 94-42438
U.S. Department of Energy
Grant DE-FG02-91-ER-54109

In advanced steady-state tokamak scenarios, a substantial fraction of the necessary plasma current will be provided by the bootstrap current. The use of radio frequency waves to generate the remainder of this current is a practical idea in steady state tokamaks. We have been studying the interaction of RF waves with the neoclassical bootstrap current.

The bootstrap current was initially predicted by the neoclassical theory of transport in toroidally shaped plasmas.[22] If we consider a plasma in the shape of a cylindrical torus, as shown in figure 8, then the confinement of this plasma by a magnetic field results in a gradient of plasma pressure inwards along the minor radius. The diffusion of particles against this gradient drives a current in the toroidal (ϕ) direction.

In a tokamak, the toroidal magnetic field is inversely proportional to the major radius R. There is also a

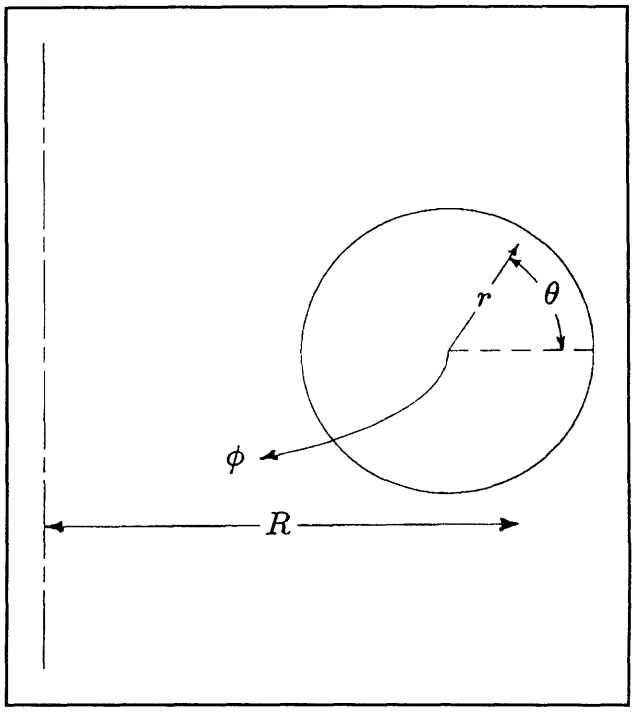

Figure 8. Toroidal coordinate system.

magnetic field in the poloidal direction, and this causes a small fraction of particles to become trapped in a magnetic well. These trapped particles are limited to the region where θ is less than a critical trapping angle θ_c, and they also have a small drift in the radial direction caused by the inhomogeneity and the curvature of the magnetic field. The orbits followed by the trapped particles are known as banana orbits. Figure 9 shows two of these orbits, labeled A and B, projected onto a poloidal cross section. The two orbits each pass through the same point X, but in opposite directions. A decrease in plasma density with increasing r means that there will be more particles on orbit A than on orbit B. Thus at point X, there will be a net current of trapped particles in both the poloidal and toroidal directions. Quantitatively, this current has a value

$$J_{\|} \sim \left(\frac{r}{R}\right)^{3/2} \frac{1}{B_\theta} \frac{dp}{dr}.$$

Neoclassical theory shows that this current will be enhanced by a factor of R/r due to collisions which transfer momentum from trapped particles to passing particles. This gives the bootstrap current.

---

[21] V. Fuchs, A.K. Ram, S.D. Schultz, A. Bers, and C.N. Lashmore-Davies, "Mode Conversion and Electron Damping of the Fast Alfvén Wave in a Tokamak at the Ion-Ion Hybrid Frequency," *Physics of Plasmas*, forthcoming.

[22] M.N. Rosenbluth, R.D. Hazeltine, and F.L. Hinton, *Phys. Fluids* 13: 116 (1972).

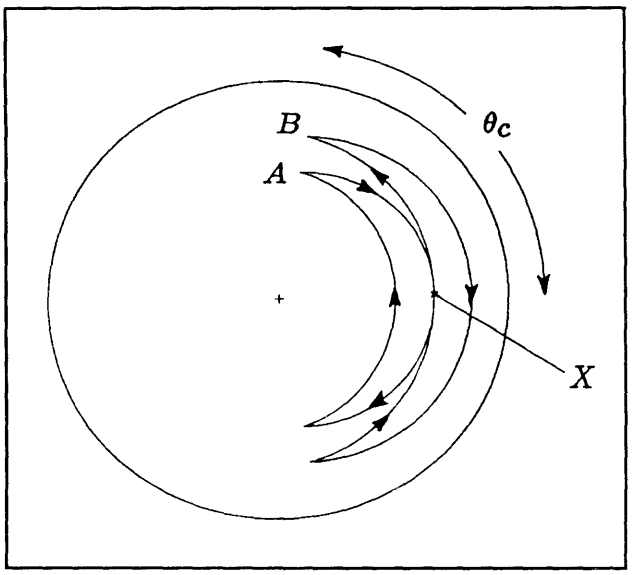

Figure 9. Poloidal cross section showing trapped particle orbits.

RF waves, used to drive a current, interact primarily with those electrons which move in resonance with the phase velocity of the waves. In this particular resonant region of velocity space, the diffusion of electrons can be modeled by a quasilinear operator.[23] In the absence of the bootstrap current, it is the balance of this quasilinear diffusion with collisions which gives the steady-state distribution of electrons in velocity space. Usually RF waves interact with tail electrons; however, they can be used to modify the bulk distribution.

The steady-state distribution function f of electrons is assumed to be averaged over the magnetic gyromotion, and, for an axisymmetric tokamak, is independent of the toroidal angle ϕ. Under these assumptions, f can be written as a function of the guiding center coordinates r and θ and two constants of the motion, the electron's energy E and magnetic moment μ. Then f will satisfy the steady-state form of the drift kinetic equation (DKE)

$$v_{\|} \frac{B_\theta}{B} \frac{1}{r} \frac{\partial f}{\partial \theta} + v_{Dr} \frac{\partial f}{\partial r} = C(f) + Q(f). \qquad (1)$$

In terms of the coordinates (E, μ, r, θ), the parallel velocity is given by

$$v_{\|}(E, \mu, r, \theta; \sigma) = \sigma \left\{ \frac{2}{m} [E - \mu B(r, \theta)] \right\}^{1/2} \qquad (2)$$

where $\sigma \equiv v_{\|}/|v_{\|}| = +1$ or -1, and the radial drift velocity is

$$v_{Dr}(E, \mu, r, \theta) = \frac{m}{eB_o} \frac{v_{\|}}{r} \frac{\partial}{\partial \theta} (h v_{\|}), \qquad (3)$$

where $h = R/R_o = 1 + (r/R_o)\cos\theta$. The current is found by taking the first-order velocity space moment of f, $J_{\|} = -e \int d^3v\, v_{\|} f$.

The DKE (1) is a partial differential equation in four dimensions, which makes finding a general solution for $f(E, \mu, r, \theta)$ complicated. One way to reduce the number of dimensions is to average over one bounce orbit in θ. This bounce average is defined as

$$\{A\} \equiv \int \frac{d\theta}{v_{\|}} A \Big/ \int \frac{d\theta}{v_{\|}} \qquad (4)$$

where the integral is taken from $\theta = -\pi$ to $+\pi$ for passing particles and from $\theta = -\theta_c$ to θ_c for trapped particles.

An approximate solution for f can be obtained by expanding in terms of two small parameters. The first of these expansion parameters is the ratio of the width of a banana orbit to the tokamak's minor radius, $\Delta_b/a \equiv \delta \ll 1$. The second parameter is the ratio of the electron collision frequency (as evaluated in the collision operator C) to the frequency of bounce orbits, $\nu_c/\omega_b \equiv \hat{\nu} \ll 1$. Expanding in these parameters, $f = f_o^{(o)} + \delta f_o^{(o)} + \hat{\nu} f_o^{(1)} + \delta \hat{\nu} f_1^{(1)} + \cdots$. Substituting this into (1) and equating terms of the same order, we get

$$v_{\|} \frac{B_\theta}{B} \frac{1}{r} \frac{\partial f_o^{(o)}}{\partial \theta} = 0 \qquad (5)$$

$$v_{\|} \frac{B_\theta}{B} \frac{1}{r} \frac{\partial f_o^{(1)}}{\partial \theta} = C(f_o^{(o)}) + Q(f_o^{(o)}) \qquad (6)$$

$$v_{\|} \frac{B_\theta}{B} \frac{1}{r} \frac{\partial f_1^{(o)}}{\partial \theta} = -v_{Dr} \frac{\partial f_o^{(o)}}{\partial r} \qquad (7)$$

$$v_{\|} \frac{B_\theta}{B} \frac{1}{r} \frac{\partial f_1^{(1)}}{\partial \theta} = C(f_1^{(o)}) + Q(f_1^{(o)}) - v_{Dr} \frac{\partial f_o^{(1)}}{\partial r}. \qquad (8)$$

[23] C.F. Kennel and F. Engelmann, *Phys. Fluids* 9: 2377 (1966).

The bounce average of (6) gives an equation for $f_0^{(o)}$:

$$0 = \{C(f_o^{(o)}) + Q(f_o^{(o)})\}. \quad (9)$$

This is the equation for the modified electron distribution due to RF effects. The bootstrap current is contained in the $f_1^{(o)}$ term, so we only solve for $f_0^{(o)}$ and $f_1^{(o)}$. From (7) and (3), we find the θ-dependent part of $f_1^{(o)}$:

$$f_1^{(o)} = \frac{-m}{eB_o} v_{\|} \frac{\partial f_o^{(o)}}{\partial r} + \tilde{f}_1^{(o)}. \quad (10)$$

Finally, to find the θ-independent quantity $\tilde{f}_1^{(o)}$, we must bounce average (8).

Alternatively, we can use the adjoint technique,[24] which may allow us to solve for the plasma current without finding all the details of the electron distribution. This technique makes use of the self-adjoint property of the linearized collision operator C in the DKE (1). For any two distribution functions f and g which are slightly perturbed from a Maxwellian f_M, the adjoint property can be written as

$$\int d^3v g f_M^{-1} C(f) = \int d^3v f f_M^{-1} C(g). \quad (11)$$

If f is the solution of (1), and we let g be the toroidal generalization of the Spitzer-Härm distribution function,[25] then we can express the parallel current in terms of g:

$$J_{\|} = \frac{-eB}{2\pi q} \int_0^{2\pi} \frac{r d\theta}{B_\theta} \int d^3v \left(\vec{S}_{RF} \cdot \frac{\partial}{\partial \vec{v}} + \frac{m}{eB_o} \frac{v_{\|}}{r} v_{\|} h \frac{\partial f}{\partial r} \frac{\partial}{\partial \theta} \right) g e^{-E/T_e}. \quad (12)$$

Although originally applied only to RF and beam driven currents, the adjoint technique has been used to predict the bootstrap current in the absence of RF waves.[26] We will use the adjoint technique to determine the effect of RF waves on the bootstrap current.

The equations discussed above can be solved analytically and numerically to study the net current produced by bootstrap in conjunction with several different types of RF waves, including lower hybrid waves, fast Alfvén waves, and electron cyclotron waves. This will allow us to predict an RF scheme which can modify the electron distribution to provide an enhanced bootstrap current. We are also in the process of solving the four-dimensional DKE in its complete form on a parallel processing machine.

1.2.3 Fast Ion Orbits in a Tokamak

Sponsor

U.S. Department of Energy
Grant DE-FG02-91-ER-54109

Ion cyclotron heating in a two ion-species plasma increases the perpendicular energy of resonant minority ions as experimental evidence shows.[27] As these particles gain energy, they also become increasingly trapped in the magnetic field of a tokamak. The particles are being scattered into the trapped region as pitch-angle scattering is not fast enough to scatter the particles back in the passing region. Resonant ions can become so energetic that their orbits touch the plasma edge and their banana widths reach dimensions comparable to the minor radius. The banana tips move toward the resonant layer as they gain perpendicular energy when they cross the resonant layer. To understand the transport of these energetic particles due to RF

[24] S.P. Hirshman, *Phys. Fluids* 23: 1238 (1980); T.M. Antonsen, Jr. and K.R. Chu, *Phys. Fluids* 25: 1295 (1982).

[25] L. Spitzer and R. Härm, *Phys. Rev.* 89: 977 (1953).

[26] Y.R. Lin-Liu, F.L. Hinton, C.F.F. Karney, and S.P. Hirshman, "A Numerical Study of the Neoclassical Bootstrap Current Using Adjoint Functions," *Proceedings of the International Sherwood Fusion Theory Conference,* Dallas, Texas, March 14-16, 1994, paper 3C37; O. Sauter, Y.R. Lin-Liu, F.L. Hinton, and J. Vaclavik, CRPP Report LRP 503/94, p. 41 (1994).

[27] J. Hosea, *Phys. Rev. Lett.* 43: 1802 (1979).

and collisions, their orbits need to be known in detail.[28] We restrict this study to barely-confined trapped particles that touch the plasma edge. These particles are mainly responsible for fast density and energy loss to the plasma wall. We label these particles by the position of their banana tips.

We work in a tokamak cross section where the radial coordinate is $x = r/a$ and the poloidal coordinate is θ. a is the tokamak minor radius, while the major radius is given by R_0. The geometric factor is $h = 1 + x\frac{a}{R_0}\cos\theta$. The parallel and perpendicular velocities of a particle are respectively $v_{\|}$ and $v_{\perp}$. An algebraic equation for particle orbits can be derived by making use of the integrals of motion. These are the energy, the magnetic moment and the toroidal momentum, given respectively by equations (1), (2) and (3):

$$\bar{v}^2 = \frac{v^2}{v_{th}^2} \tag{1}$$

$$\bar{\mu} = h\bar{v}_{\perp}^2 \tag{2}$$

$$\bar{p} = -h\bar{v}_{\|} + A_c x^2 \tag{3}$$

where the parameter A_c is defined as follows

$$A_c = \frac{\mu_0 q I}{4\pi m v_{th}} \tag{4}$$

where I is the total plasma current. We solve for $\bar{v}_{\|}$ using (1) and (2), and substitute it into the expression for the toroidal momentum to get an equation in θ and x. The orbit equation is quartic in x:

$$ax^4 + c(\theta)x^2 + d(\theta)x + e = 0 \tag{5}$$

where

$$a = A_c^2;\ c = -2\bar{p}A_c - \left(\frac{a}{R_0}\right)^2\bar{v}^2\cos^2\theta \tag{6}$$

and

$$d = \cos\theta\left(-2\frac{a}{R_0}\bar{v}^2 + \frac{a}{R_0}\bar{\mu}\right);\ e = \bar{p}^2 - \bar{v}^2 + \bar{\mu}. \tag{7}$$

The orbit equation describes all particle trajectories in a tokamak as functions of the constants of motion. We assume $\cos\theta = 1$; the orbit equation then becomes

$$ax^4 + c_1x^2 + d_1x + e = 0 \tag{8}$$

where our coefficients are

$$c_1 = -2\bar{p}A_c - \left(\frac{a}{R_0}\right)^2\bar{v}^2 \tag{9}$$

and

$$d_1 = -2\frac{a}{R_0}\bar{v}^2 + \frac{a}{R_0}\bar{\mu}. \tag{10}$$

To study the orbits of barely-confined particles, we let $x = 1$. This yields an equation for our constants of motion:

$$A_c^2 - 2\bar{p}A_c - \left(\frac{a}{R_0}\right)^2\bar{v}^2 - 2\bar{v}^2\frac{a}{R_0} + \bar{\mu}\frac{a}{R_0} + \bar{p}^2 - \bar{v}^2 + \bar{\mu} = 0. \tag{11}$$

Our choice of the constants of motion is now restricted to a two-dimensional space rather than a three-dimensional one. We can also let the inverse-aspect ratio equal one-third without too much loss of generality.

Energetic trapped particles that interact resonantly with the fast Alfvén wave eventually end up having their banana tips close to the resonant layer. These particles have a strong resonant interaction with the ion-cyclotron wave and therefore deserve careful study. They can be easily identified in phase space by looking at their constants of motion. By setting the parallel velocity of the particle at its banana tip to zero, one can easily derive the following relations for the momentum and the energy:

$$p = A_c x_0^2;\ \bar{v}^2 = \bar{\mu} \tag{12}$$

where x_0 is the radial coordinate of the banana tip of the trapped particle. By substituting these relations in the orbit equation we get:

$$A_c^2 - 2A_c^2x_0^2 - \frac{4\bar{v}^2}{9} + A_c^2x_0^4 = 0. \tag{13}$$

[28] T.E. Stringer, *Plas. Phys.* 16: 651 (1973); J. Rome and Y.K.M. Peng, *Nuclear Fusion* 19: 1193 (1979).

Solving for x_δ^2:

$$x_{01}^2 = 1.0 + \frac{1}{3A_c/2}\sqrt{\bar{v}^2} \tag{14}$$

and

$$x_{02}^2 = 1.0 - \frac{1}{3A_c/2}\sqrt{\bar{v}^2}\,. \tag{15}$$

The first root $x_{\delta 1}^2$ can be discarded because it gives a trajectory that goes outside the torus on the resonance layer. Solving (15) for the energy, we obtain:

$$\bar{v}^2 = \frac{9}{4}A_c^2(1 - x_0^2)^2. \tag{16}$$

The energy has been normalized to 1 KeV. We are interested in particles whose energies are well above the thermal energy. One can observe that the most energetic trapped particles have their tips close to the center of the plasma. As the energy decreases, the tips move radially outward along the resonance layer. The maximum energy that such particles can have while still being confined is 1.2 MeV. In general, the maximum energy is determined by the toroidal current flowing in the tokamak. The maximum confined energy scales approximately as the total current squared.

We now generalize the approach which we took to study the trapped particles whose tips touch the resonant layer. We let the parallel velocity be equal to zero at some point and compute the constants of the motion as functions of the coordinate of this point. Doing so, we obtain

$$\bar{\mu} = \left(1 + \frac{1}{3}\cos\theta_0 x_0\right)\bar{v}^2;\ \bar{p} = A_c x_0^2 \tag{17}$$

where x_0 and θ_0 are the radial and poloidal angle coordinates of the tip of the banana. By substituting these expressions into (16) we obtain:

$$\bar{v}^2 = \frac{9}{4}A_c^2\frac{(x_0^2 - 1)^2}{1 - x_0\cos\theta_0}\,. \tag{18}$$

These expressions allow us to find the constants of motion given the location of the banana tips.

We are studying barely-confined trapped particles in phase space. We have shown that the location of their tips is the most convenient phase space label to study the orbits of these particles. Passing particles are not included in this analysis because only a small fraction of these particles are barely-confined. In the future, we will discuss the effect that the fast Alfvén wave and collisions have on the unperturbed orbits.

1.2.4 Publications

Bers, A. "Simple Physics of LH $k_{\|}$ Upshift Due to Density Gradient Along $\vec{B}_0$." *Proceedings of the U.S.-Japan Workshop on RF Heating and Current Drive*, MIT Plasma Fusion Center, Cambridge, Massachusetts, November 15-17, 1994.

Bers, A., A.K. Ram, and C.C. Chow. "Saturation of SRS by Spatiotemporal Chaos in Coupled Langmuir Decay." *Bull. Amer. Phys. Soc.* 39: 1754 (1994).

Chan, K.P. *Stochasticity Induced by Electrostatic Waves in Magnetized Plasma.* S.M. thesis. Dept. of Electr. Eng. and Comput. Sci. and Dept. of Physics, MIT, 1994.

Chow, C.C., A.K. Ram, and A. Bers. "Saturation of SRS by Spatiotemporal Chaos in Coupled Langmuir Decay." Revised Report PFC/JA-94-8-REV. Cambridge, Massachusetts: MIT Plasma Fusion Center, 1994.

Delcroix, J.L., and A. Bers. *Physique des Plasmas.* Vols. 1 and 2. Paris, France: InterÉditions/ CNRS Éditions, 1994.

Fuchs, V., A.K. Ram, S.D. Schultz, A. Bers, and C.N. Lashmore-Davies. "Mode Conversion and Electron Damping of the Fast Alfvén Wave in a Tokamak at the Ion-Ion Hybrid Frequency." CCFM Report RI 447e. Quebec, Canada: Centre Canadien de Fusion Magnétique, October 1994.

Fuchs, V., S.D. Schultz, A.K. Ram, A. Bers, and C.N. Lashmore-Davies. "Mode Conversion of the Fast Alfvén Wave in a Tokamak at the Ion-Ion Hybrid Frequency." *Bull. Amer. Phys. Soc.* 39: 1627 (1994).

Ram, A.K., and A. Bers. "Hamiltonian Chaos in Wave-Particle Interactions." Invited paper presented at the 1993 Cambridge Workshop on Theoretical Geoplasma Physics. In *Physics of Space Plasmas, SPI Conference Proceedings and Reprint Series Number 13.* Eds. T. Chang and J.R. Jasperse. Cambridge, Massachusetts: Scientific Publishers, 1993.

Ram, A.K., and A. Bers. "Hamiltonian Chaos in Wave-Particle Interactions." Report

PFC/JA-94-22. Cambridge, Massachusetts: MIT Plasma Fusion Center, 1994.

Ram, A.K., A. Bers, V. Fuchs, and S.D. Schultz. "Current Drive by the Combination of Lower Hybrid and ICRF Waves." *Proceedings of the 21st European Physical Society Conference on Controlled Fusion and Plasma Physics,* Montpellier, France, June 27 - July 1, 1994. 3: 1134-1137 (1994).

Ram, R.K., A. Bers, V. Fuchs, and S.D. Schultz. "Current Drive by the Combination of Lower Hybrid and ICRF Waves." Report PFC/JA-94-18. Cambridge, Massachusetts: MIT Plasma Fusion Center, 1994.

Ram, A.K., A. Bers, V. Fuchs, and S.D. Schultz. "Enhanced Current Drive with Lower-Hybrid and Ion-Bernstein Waves." *Proceedings of the 15th International Atomic Energy Agency Conference on Plasma Physics and Controlled Nuclear Fusion,* Seville, Spain, September 26 - October 1, 1994. Vienna, Austria: IAEA. Paper IAEA-CN-60/D-P-I-15. Forthcoming.

Ram, A.K., A. Bers, V. Fuchs, and S.D. Schultz. "Enhanced Current Drive with Lower-Hybrid and Ion-Bernstein Waves." Report PFC/JA-94-34. Cambridge, Massachusetts: MIT Plasma Fusion Center, 1994.

Ram, A.K., A. Bers, V. Fuchs, and S.D. Schultz. "Enhancing Lower Hybrid Current Drive Efficiency with Fast Alfvén Waves and Ion-Bernstein Waves." 7th Boulder International RF Advanced Tokamak Workshop, Boulder, Colorado, April 6-8, 1994.

Ram, A.K., A. Bers, V. Fuchs, and S.D. Schultz. "Enhancing Lower Hybrid Current Drive with ICRF Waves." *Proceedings of the International Sherwood Fusion Conference,* Dallas, Texas, March 14-16, 1994. Paper 1C49.

Ram, A.K., A. Bers, V. Fuchs, and S.D. Schultz. "Heating and Current Drive by Mode-Converted Ion-Bernstein Waves." *Proceedings of the U.S.-Japan Workshop on RF Heating and Current Drive,* MIT Plasma Fusion Center, Cambridge, Massachusetts, November 15-17, 1994.

Ram, A.K., A. Bers, S.D. Schultz, and V. Fuchs. "Interaction of Ion-Bernstein Waves with Electrons." *Bull. Amer. Phys. Soc.* 39: 1626 (1994).

Ram, A.K., C.C. Chow, and A. Bers. "Saturation of SRS by Spatiotemporal Chaos in Coupled Langmuir Decay." *Proceedings of the 21st European Physical Society Conference on Controlled Fusion and Plasma Physics,* Montpellier, France, June 27 - July 1, 1994, 3: 1460-1463 (1994).

Schultz, S.D., A. Bers, and A.K. Ram. "Effect of RF Waves on Bootstrap Current in Tokamaks." *Bull. Amer. Phys. Soc.* 39: 1625 (1994).

1.3 Physics of Thermonuclear Plasmas

Sponsor

U.S. Department of Energy
Contract DE-FGO2-91ER-54109

Project Staff

Professor Bruno Coppi, Dr. Giuseppe Bertin, Dr. Francesca Bombarda, Franco Carpignano, William S. Daughton, Dr. Paolo Detragiache, Darin R. Ernst, Andrew J. Kerman, Catherine Lorusso, Dr. Stefano Migliuolo, Gregory E. Penn, Darren M. Pierre, Caterina Riconda, Todd H. Rider, Suraj D. Salihu, Dr. Linda E. Sugiyama, George M. Svolos, Miriam Weiner

As our primary activity in this research program, we study the physics of magnetically confined plasmas in regimes relevant to present-day advanced experiments on high-temperature plasmas and to near-future thermonuclear reactors. The main objective of these experiments is to bring the plasma ("thermonuclear fuel") produced in toroidal magnetic confinement configurations to ignition conditions. The first generation fuel consists of deuterium-tritium mixtures (considered for the Ignitor and ITER experimental programs), and this should be followed by experiments with more advanced fuels such as deuterium-deuterium or deuterium-helium mixtures that have a lower rate of neutron production (CANDOR program).

The Ignitor-Ult machine is now in the early stages of construction in Europe. At MIT, the Alcator C-MOD experiment combines the favorable features of an elongated plasma cross section with a high magnetic field to produce high-plasma currents and sustain high-plasma densities with the high degree of purity that is required for fusion reactors. This is, in fact, consistent with a research program that we had formulated in the early 1970s with the proposal of a high-field, elongated plasma machine called Megator. Megator was capable of producing megampere plasma currents in a compact configuration. The Megator concept, with similar parameters to those of Alcator C-MOD, had been studied

as a logical evolution of the Alcator program that had been established at MIT since 1989.

First, the basic physical processes that characterize the properties and the dynamics of thermonuclear plasmas are being studied as they apply to existing or near-term future systems. In this effort, we closely collaborate with our experimental colleagues, as well as theorists from other research groups (e.g., Columbia, JET, Phillips Laboratory, Princeton, University of Texas, Lawrence Livermore National Laboratories). This work also involves time-dependent simulations of plasma discharges in the Ignitor-Ult experiment. We focus particular attention on the evolution of spatial profiles of plasma current and temperature. Collaboration with our colleagues at the E.N.E.A. laboratories of Italy (Ente per le Nuove Tecnologie, l'Energia e l'Ambiente), as well as in-house code development, plays a major role in this endeavor.

Second, we explore advanced regimes of thermonuclear burning, including those employing low neutron yield fuels (D-^{3}He, and "catalyzed" D-D). We consider both the design of machines that will contain these very high temperature plasmas as well as the physics that govern their behavior. Below, we discuss some salient results of work completed or presently being carried out by members of our research group.

1.3.1 Isotopic Effect in Transport and the Ubiquitous Mode

We have investigated the linear stability of the collisionless trapped electron mode (first called "the ubiquitous mode")[29] in plasmas with two or more ion species. In addition to this mode, whose perturbed electrostatic potential has even-parity about the midplane of the torus $\phi(-\theta) = \phi(\theta)$, the toroidal ion temperature gradient (ITG) mode with odd-parity is also investigated.[29] The calculations are performed in a low-β toroidal geometry. Two L-mode discharges in the JET and TFTR experiment are used to provide reference parameters for this study.[30] This work is carried out in the intermediate frequency regime, $k_{\|}v_{Ti} \ll \omega \ll k_{\|}v_{Te}$, appropriate to describe the perturbations that are observed to dominate the spectrum in poloidal wavenumber (i.e., those with $k_\theta v_{Ti}/\omega_{ci} \sim 1$).[31]

The linear stability analysis shows that the $\gamma(k_\theta)$ spectrum has no maximum in the regime of interest, $\partial\gamma/\partial|k_\theta| > 0$, and that the presence of an impurity ion species leads to a moderate decrease in the growth rate (at constant poloidal wavenumber), simply due to an effect of dilution of the primary (hydrogenic) ion: $n_i = n_e - Z_i n_i$. This holds true for both even-parity (ubiquitous) and odd-parity (ITG) modes. An important detail to remember is that this stabilization exhibits no particular scaling with isotopic mass; indeed the stabilizing trend saturates quite quickly (around $A_i \sim 12$, i.e., carbon) and is a stronger function of impurity charge concentration ($Z_i n_i$).

The realization that the single-ion dispersion relation is a function of a set of parameters where mass and charge occur only in the Larmor radius, $\rho_i \propto A_i/Z_i$, leads to the realization that a change in the ion species constituting the thermonuclear fuel (for instance, from Deuterium to Tritium) automatically entails a shift of the linear wave spectrum, in poloidal wavenumber, so that $k_\theta\rho_i$ remains constant. We speak of "poloidal wavenumber" only for convenience. In reality, many poloidal harmonics are coupled toroidally to create the unstable eigenmode in our analysis (carried out via the "ballooning representation"). The one true "quantum number" here is the toroidal wavenumber, n, so that $k_\theta = nq(r_s)/r_s$ where r_s is the radius of the reference rational surface and $q = rB/RB_\theta$. This conclusion in turn makes any model that relies on a mixing length formula, $D \propto \gamma/k_\theta^2$, exhibit an anti-isotopic effect whereby transport (measured by the particle diffusion coefficient D) increases with isotopic mass, in contradiction with experimentally observed trends.

The resolution lies apparently in adopting a description in which turbulence in experiments (e.g., JET)[32] where an isotopic effect is observed ($D \propto A_i^{-1/2}$) is mostly determined by the quasilinear spectrum of linearly unstable modes. A simple calculation then shows that the quasilinear particle flux is due to the quasi-circulating electrons (the ones that have undergone drift-reversal), for cases with

---

[29] B. Coppi and F. Pegoraro, *Nucl. Fusion* 17: 969 (1977).

[30] S. Migliuolo, "Isotropic Effect in Transport and the Ubiquitous Mode," *Phys. Lett. A* 198: 341 (1995).

[31] R.J. Fonck, G. Cosby, R.D. Durst, S.F. Paul, N. Bretz, S. Scott, E. Synakowski, and G. Taylor, *Phys. Rev. Lett.* 70: 3736 (1993).

[32] F. Tibone, B. Balet, M. Bures, J.G. Cordey, T.T.C. Jones, P.J. Lomas, K. Lawson, H.W. Morsi, P. Nielsen, D.F.H. Start, A. Tanga, A. Taroni, K. Thomsen, and D.J. Ward, *Nucl. Fusion* 22: 413 (1993).

standard profiles ($\nabla T \cdot \nabla n > 0$), and that this flux is of the type:

$$\Gamma = 2\sqrt{\pi}\,\frac{cT_e}{eB}\sum_{k_\theta} k_\theta \Gamma_k$$

where Γ_k is a function of dimensionless variables that are invariant under isotopic substitution (for constant density and temperature profiles). This then leads, in a natural fashion, both to the isotopic effect (D decreasing with isotopic mass) as well as to the inverse dependence on charge, specifically $D \propto Z$ in this model. We note that the first theoretical model[33] to explain the observation of the isotopic effect was based on the excitation of third species ("impurity") driven modes at the edge of the plasma column.

1.3.2 Ideal-MHD Stability of Ignition Experiments

We have undertaken a study of the linear stability of toroidal plasmas in fully shaped toroidal configurations (i.e., including effects due to finite aspect ratio, ellipticity and triangularity) in parameter regimes relevant to ignition experiments, such as Ignitor and ITER. The analysis is carried out within the ideal magnetohydrodynamic (MHD) approximation, using the numerical equilibrium and stability code PEST-1 developed at Princeton University.[34] The input pressure and q profiles are taken in accordance with ITER design specifications and transport modeling:

$$P(\psi) = P_0(1-\psi)^{3/2} \qquad q(\psi) = q_0 + (q_a - q_0)\psi^3$$

Computations indicate that a pressure driven internal mode is unstable, with low threshold value (~ 1) in the parameter $\beta_N \equiv \beta(\%)a(m)B(T)/I_p(MA)$, where $\beta = 8\pi < p > /B^2$ and $< p >$ is the volume averaged plasma pressure. This is in agreement with practically all other stability analyses that have been carried out with $q_0 < 1$.

As is well known,[35] the physical parameter of relevance is β_p, the poloidal beta averaged within the $q \leq 1$ volume, and Ignitor is designed to operate at values of this parameter that are below critical ($\beta_p^{crit} \sim 0.3$). ITER, on the other hand, does not have this "safety feature" in its design and we expect it to be subject to an ideal MHD instability, which may lead to either large sawteeth, reconnection, and/or disruptions. A sample curve of the normalized growth rate as a function of $\beta(\%)$ is shown in figure 10. These instabilities are not amenable to wall stabilization, owing to their internal nature. The eigenfunction is dominated by the m=1,2 poloidal harmonics which mostly affect the $q \leq 2$ volume. See figure 11, we fix the toroidal mode number n=1; this is the most unstable case. Since this volume encompasses nearly 75 percent of the plasma, these modes which tend to mix the plasma via a macroscopic convective cell are likely to be extremely detrimental to the fusion reactivity in the experiments.

In addition, it should be noted that fast particle stabilization, by fusion α-particles, will not be effective in ITER. On the contrary, a preliminary calculation performed in collaboration with F. Porcelli from the Politechnic of Turin, indicates that the energy content in the α population is large enough to cause the appearance of the trapped particle branch of the fishbone. This is the high frequency[36] counterpart of the resonant m=1 oscillation[37] that is responsible for the scattering and ejection from the plasma of energetic ions in neutral beam-heated experiments.

Finally, we note that ignition experiments operate in regimes that are more collisional than present-day high temperature devices such as JET and TFTR and, in the case of Ignitor, with thermal plasmas. Thus, the physics of reconnecting modes[38] will be important and the subject of future study.

---

[33] B. Coppi, in *Plasma Physics and Controlled Nuclear Fusion Research*, (Vienna: I.A.E.A., 1991).

[34] R.C. Grimm, R.L. Dewar, and J. Manickam, *J. Comp. Phys.* 4: 94 (1983).

[35] M.N. Bussac, R. Pellat, D. Edery, and J.L. Soulé, *Phys. Rev. Lett.* 35: 1638 (1975); L.E. Zakharov, *Sov. J. Plasma Phys.* 4: 503 (1978); A.C. Coppi and B. Coppi, *Nucl. Fusion* 32: 205 (1992).

[36] L. Chen, R.B. White, and M.N. Rosenbluth, *Phys. Rev. Lett.* 52: 1122 (1984).

[37] B. Coppi and F. Porcelli, *Phys. Rev. Lett.* 57: 2272 (1986).

[38] G. Ara, B. Basu, B. Coppi, G. Laval, M.N. Rosenbluth, and B.V. Waddell, *Ann. Phys.* 112: 443 (1978).

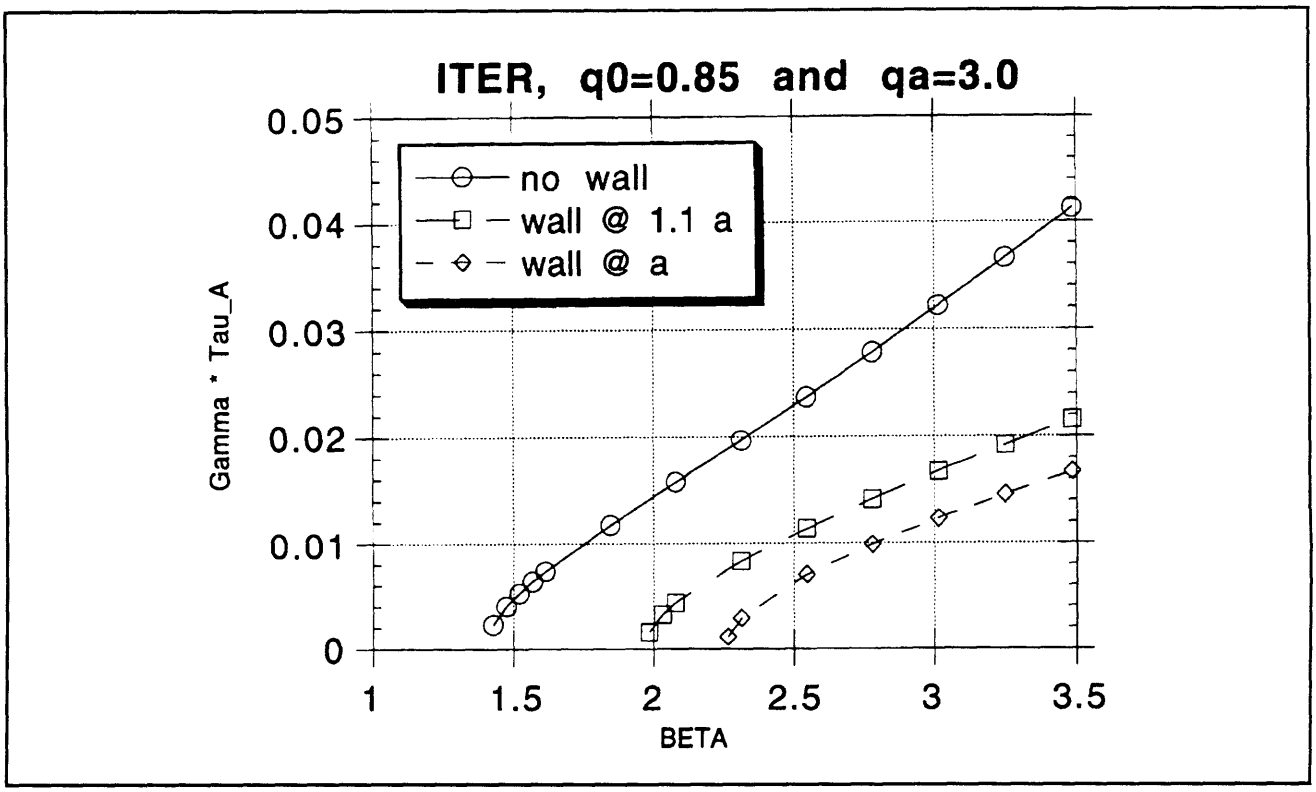

Figure 10.

1.3.3 Analysis of Disruptions in the TFTR Experiment

Disruptions (i.e., the sudden loss of control of the plasma, followed by a quench of the current and termination of the discharge) are a serious problem in toroidal magnetic confinement experiments. Disruptions limit the regime of operation (either in density, current, or pressure) and can have deleterious effects on the structural integrity of the Tokamak vacuum vessel due to the electromotive forces induced by the disruption.

In collaboration with Professor Jeffrey P. Freidberg, Dr. Jay Kesner, and Dr. Jesus Ramos we have begun an analysis of the plasma properties leading to disruption in the TFTR experiment at Princeton University. We have concentrated on events where pressure played a role such as the so-called "beta limit", where the plasma is unable to exceed a maximum value in the parameter $\beta = 8\pi < p > /B^2$, the ratio of the volume averaged plasma pressure to the magnetic field energy density. The parameter of merit, $\beta_N = \beta(\%)B(T)a(m)/I(MA)$, rarely reaches the expected maximum value (~ 3) in TFTR. Instead, a macroscopic phenomenon appears around $\beta_N \sim 2$ to limit the discharge.

Our original goal was to understand the physical cause of these disruptions and to deduce a cure for the relatively low values of β_N in TFTR. While this remains a major objective of our project, our work has pointed to an apparent major problem in the use of ideal-MHD linear stability codes as predictive tools for the TFTR tokamak, as well as, probably, other auxiliary heated experiments with substantial nonthermal populations of ions. The numerical codes predict the appearance of pressure-driven modes (with toroidal number n=1) well before any external manifestation occurs in the experiment. This occurs in the analysis of TFTR discharges where $q(0) < 1$, and it has been reported also to be the case for DIII-D plasmas.[39] The numerical analysis predicts the appearance of a linearly unstable mode whose dominant poloidal component is m=1 and with measurable m=2,3 components present due to toroidal coupling. Among the discharges analyzed was a high power shot 76778 (at the time, record) which achieved 10 MW fusion power. A careful modeling, employing $p(\psi)$ and $q(\psi)$ profiles, where $0 \leq \psi \leq 1$ is the normalized poloidal flux,

[39] T. Taylor, private communication.

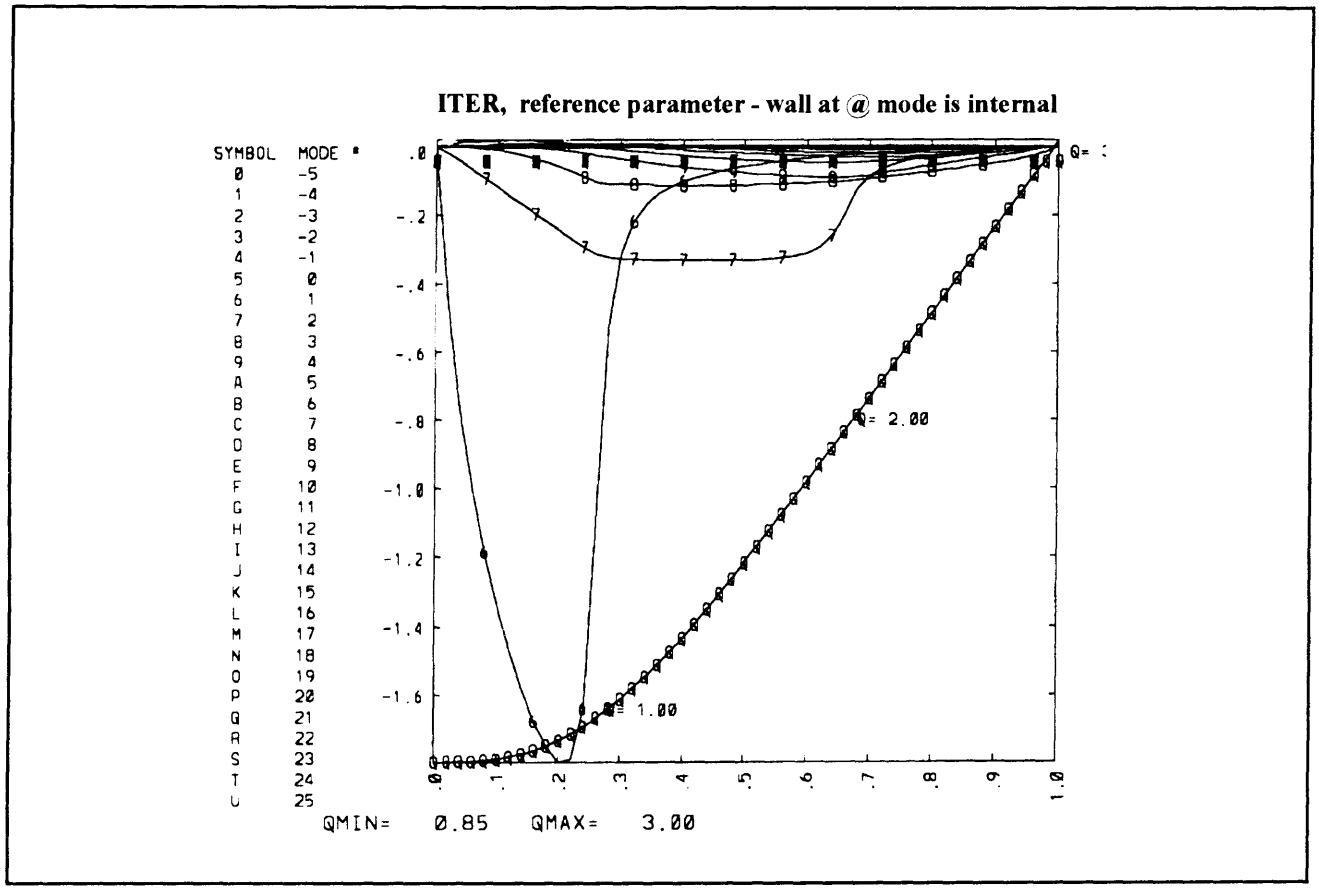

Figure 11.

obtained from TRANSP was performed using both PEST-1 and PEST-2 stability codes with the aforementioned results.

Resolutions of this apparent discrepancy are being sought at this time. They include the role of so-called "FLR stabilization" due to finite ion diamagnetic frequency either in the linear or nonlinear[40] regimes as well as other effects that involve breaking the single-fluid approximation.

Ongoing analysis includes discharges involving plasmas without a q=1 surface. These configurations involve reversed magnetic shear profiles, e.g., $q(0) > 2$, $q_{min} < 2$, and $q(a) \sim 5 - 6$. In those cases, an n=1 and (dominant) m=2 appears at sufficiently high pressures. At present, results are mixed, with the linear code underestimating threshold in some cases, relative to the value of β_N at the time of the disruption, and overestimating in others. Apparently, the problem resides in the fact that the q-profiles are known with less accuracy in these instances (and the value of q_{min} is crucial for the analysis) rather than in the presence of additional physics.

1.3.4 Emissions at the Harmonics of the Cyclotron Frequency

An important source of information on the distribution of α-particles in DT fusion plasmas is the spectrum of radiation emission in the range of the α-particle cyclotron frequency and above.

Localized magnetosonic-whistler modes are thought to lie[41] behind this emission, observed in JET[42] and

---

[40] L. Zakharov, J. Manickam, W. Park, and B. Rogers, "Sawtooth Stabilization and Triggering of High-Beta Disruptions in TFTR," International Sherwood Theory Conference, Incline Village, Nevada, 1995.

[41] B. Coppi, *Phys. Lett. A* 172: 439 (1993).

[42] G.A. Cottrell et al., *Nuc. Fusion* 33: 1365 (1993).

TFTR.[43] These modes would interact resonantly with the harmonic of the α-particle cyclotron frequency, giving rise to a growth rate.

We have extended our previous work on the subject by studying the spatial structure of the magnetosonic-whistler wave.[44] We found that two classes of toroidal modes exist within the part of the spectrum where the whistler contribution is significant. One class is radially localized within a narrow shell near the outer edge of the plasma column. The distance of the shell from the axis of symmetry is found to be close to that estimated from the experiments.[42] The other class propagates almost perpendicularly to the magnetic field and can extend radially to well inside the plasma column.

Moreover, we have investigated the effects related to the inhomogeneity of the magnetic field on the instability, particularly how the growth rate is affected by toroidicity[45] for frequencies at or above the ion cyclotron frequency in the resonant case (i.e., $\omega \sim p\Omega_\alpha$).

We are now in the process of studying how the nature of the interaction is sensitive to the type of orbits along which the resonant particle travels, since we found that only trapped particles can reach the resonance region.

---

[43] S. Cauffman and R. Majeski, *Rev. Sc. Instrum.* 66: 819 (1995).

[44] B. Coppi, *Phys. Lett. A* 172: 439 (1993); C. Riconda, B. Coppi, and N. Asherie, "Spatial Structure of Magnetosonic Whistler Eigenmodes in Cylindrical Geometry," *Bull. Am. Phys. Soc.* 39: 1553 (1994).

[45] C. Riconda, B. Coppi, and G. Penn, "Emission above the Ion Cyclotron Frequency in a Nonhomogeneous Magnetic Field," International Sherwood Conference, Incline Village, Nevada, 1995.